

# High-performance $\text{LiNi}_{0.8}\text{Mn}_{0.1}\text{Co}_{0.1}\text{O}_2$ cathode by nanoscale lithium sulfide coating via atomic layer deposition

X. Wang, X. Xiao

To be published in "JOURNAL OF ENERGY CHEMISTRY"

June 2022

Photon Sciences

**Brookhaven National Laboratory**

**U.S. Department of Energy**

USDOE Office of Science (SC), Basic Energy Sciences (BES) (SC-22)

Notice: This manuscript has been authored by employees of Brookhaven Science Associates, LLC under Contract No. DE-SC0012704 with the U.S. Department of Energy. The publisher by accepting the manuscript for publication acknowledges that the United States Government retains a non-exclusive, paid-up, irrevocable, world-wide license to publish or reproduce the published form of this manuscript, or allow others to do so, for United States Government purposes.

## **DISCLAIMER**

This report was prepared as an account of work sponsored by an agency of the United States Government. Neither the United States Government nor any agency thereof, nor any of their employees, nor any of their contractors, subcontractors, or their employees, makes any warranty, express or implied, or assumes any legal liability or responsibility for the accuracy, completeness, or any third party's use or the results of such use of any information, apparatus, product, or process disclosed, or represents that its use would not infringe privately owned rights. Reference herein to any specific commercial product, process, or service by trade name, trademark, manufacturer, or otherwise, does not necessarily constitute or imply its endorsement, recommendation, or favoring by the United States Government or any agency thereof or its contractors or subcontractors. The views and opinions of authors expressed herein do not necessarily state or reflect those of the United States Government or any agency thereof.

# High-performance $\text{LiNi}_{0.8}\text{Mn}_{0.1}\text{Co}_{0.1}\text{O}_2$ cathode by nanoscale lithium sulfide coating via atomic layer deposition

Xin Wang<sup>a</sup>, Jiyu Cai<sup>a,b</sup>, Yang Ren<sup>c</sup>, Mourad Benamara<sup>d</sup>, Xinwei Zhou<sup>e</sup>, Yan Li<sup>f,g</sup>, Zonghai Chen<sup>b</sup>, Hua Zhou<sup>c</sup>, Xianghui Xiao<sup>h,\*</sup>, Yuzi Liu<sup>e,\*</sup>, Xiangbo Meng<sup>a,\*</sup>

<sup>a</sup> *Department of Mechanical Engineering, University of Arkansas, Fayetteville, AR 72701, USA*

<sup>b</sup> *Chemical Sciences and Engineering Division, Argonne National Laboratory, Lemont, IL 60439, USA*

<sup>c</sup> *The Advanced Photon Source, Argonne National Laboratory, Lemont, IL 60439, USA*

<sup>d</sup> *Institute for Nanoscience and Engineering, University of Arkansas, Fayetteville, AR 72701, USA*

<sup>e</sup> *Center for Nanoscale Materials, Argonne National Laboratory, Lemont, IL 60439, USA*

<sup>f</sup> *Institute of High Energy Physics, Chinese Academy of Sciences, Beijing 100049, China*

<sup>g</sup> *University of Chinese Academy Sciences, Beijing 100049, China*

<sup>h</sup> *National Synchrotron Light Source II, Brookhaven National Laboratory, Upton, NY 11973, USA*

\*Corresponding authors.

*E-mail addresses:* [xbmeng@uark.edu](mailto:xbmeng@uark.edu) (X. Meng), [yuziliu@anl.gov](mailto:yuziliu@anl.gov) (Y. Liu), [xiao@bnl.gov](mailto:xiao@bnl.gov) (X. Xiao)

## Abstract

The commercialization of nickel-rich  $\text{LiNi}_{0.8}\text{Mn}_{0.1}\text{Co}_{0.1}\text{O}_2$  (NMC811) has been hindered by its continuous loss of practical capacity and reduction in average working voltage. To address these issues, surface modification has been well-recognized as an effective strategy. Different from the coatings reported in literature to date, in this work, we for the first time report a sulfide coating, amorphous  $\text{Li}_2\text{S}$  via atomic layer deposition (ALD). Our study revealed that the conformal nano- $\text{Li}_2\text{S}$  coating shows exceptional protection over the NMC811 cathodes, accounting for the dramatically boosted capacity retention from  $\sim 11.6\%$  to  $\sim 71\%$  and the evidently mitigated voltage reduction from 0.39 to 0.18 V after 500 charge-discharge cycles. In addition, the  $\text{Li}_2\text{S}$  coating remarkably improved the rate capability of the NMC811 cathode. Our investigation further revealed that all these beneficial effects of the ALD-deposited nano- $\text{Li}_2\text{S}$  coating lie in the following aspects: (i) maintain the mechanical integrity of the NMC811 electrode; (ii) stabilize the NMC electrode/electrolyte interface; and (iii) suppress the irreversible phase transition of NMC structure. Particularly, this study also has revealed that the nano- $\text{Li}_2\text{S}$  coating has played some unique role not associated with traditional non-sulfide coatings such as oxides. In this regard, we disclosed that the  $\text{Li}_2\text{S}$  layer has reacted with the released  $\text{O}_2$  from the NMC lattices, and thereby has dramatically mitigated electrolyte oxidation and electrode corrosion. Thus, this study is significant and has demonstrated that sulfides may be an important class of coating materials to tackle the issues of NMCs and other layered cathodes in lithium batteries.

**Keywords:** Nickel-rich cathodes; Atomic layer deposition; Lithium sulfide; Microcracking; Phase transition; Interfacial reactions

## 1. Introduction

State-of-the-art lithium-ion batteries (LIBs) are insufficient in multiple aspects to meet the needs for the electrification of the transportation system. To this end, next-generation LIBs are undergoing intensive investigation. As part of the solutions, high-capacity and high-voltage lithium nickel manganese cobalt oxides ( $\text{LiNi}_x\text{Mn}_y\text{Co}_z\text{O}_2$ ,  $x + y + z = 1$ , i.e., NMCs) are very promising to meet the demanding energy density requirement for automobile batteries; particularly, Ni-rich NMCs ( $x \geq 0.6$ ) have attracted significant amount of attention primarily due to their cost-effectiveness and high capacity [1-3]. However, NMC cathodes commonly have been suffering from some formidable issues, such as Li/Ni cation mixing [4], irreversible layer-spinel-rocksalt phase transition [5], oxygen evolution [5, 6], microcracking [7, 8], and transition metal (TM) ions dissolution [9]. These issues are interconnected and jointly result in cell performance degradation. In particular, the higher the Ni content, the more severe the NMC cathodes' issues. Currently, the NMCs with  $x \leq 0.6$  have been successfully commercialized while  $\text{LiNi}_{0.8}\text{Mn}_{0.1}\text{Co}_{0.1}\text{O}_2$  (NMC811) is slowly paving its way into automobile batteries.

Aimed at addressing these afore-stated issues of NMCs, a variety of strategies has been investigated, such as surface modification [10-14], elemental doping [15-17], and electrolyte additives [18-20]. Among them, surface modification has been proved being a facile and effective strategy. Wet chemistry has been widely used to apply coatings on NMC powders but could not control the coating quality and remove undesired residuals completely [21]. In the past decade, atomic layer deposition (ALD) has emerged as a vapor-phase alternative to wet chemical methods, which uniquely enables high-quality conformal and uniform films over either electrode powders or prefabricated electrodes [22-24]. In addition, ALD features its low process temperature (e.g.,  $\leq 200$  °C) and accurate controllability over film growth for desirable crystallinity and thickness at

the atomic level [22-24]. To date, many different coatings have been reported to modify NMCs via wet chemistry and ALD, including oxides (e.g., Al<sub>2</sub>O<sub>3</sub> [25, 26], TiO<sub>2</sub> [27, 28], WO<sub>3</sub> [29], ZrO<sub>2</sub>, [14] Co<sub>3</sub>O<sub>4</sub> [30], and lithium metal oxides [31-34]), phosphates [35], and fluorides [36, 37]. Some most promising surface coatings and their effects on the performance of Ni-rich NMCs have been included in [Table S1 in the Supporting Information](#). Despite all these efforts documented in literature, sulfides as an important class of materials have to date not been investigated as surface coatings. One major reason may lie in the air-sensitive nature of most sulfides and thereby the difficulty to handle them safely.

Inspired by our previous experience in synthesizing the air-sensitive Li<sub>2</sub>S via ALD [38] and by the fact that Ni-rich NMCs slowly release lattice oxygen when charged to a relatively high potential (e.g.,  $\geq 4.3$  V), in this study, we made a bold attempt to investigate Li<sub>2</sub>S as a surface coating to tackle the issues of NMC811. We hypothesized that the reactivity of the Li<sub>2</sub>S surface coating to oxygen (i.e., O<sub>2</sub>) would produce some extra benefits in protecting NMC cathodes. Very interestingly, this study did verify our hypothesis and revealed some unusual benefits with the Li<sub>2</sub>S surface coating, as illustrated in [Fig. 1](#). The nanoscale Li<sub>2</sub>S coating was conformally coated on prefabricated NMC811 electrodes ([Fig. 1a](#)) directly at a low process temperature 150 °C. The resultant Li<sub>2</sub>S-coated NMC electrode ([Fig. 1b](#)) is enlarged in [Fig. 1\(c\)](#). We speculated that, during charge processes, the released O<sub>2</sub> from the NMC lattices would react with the Li<sub>2</sub>S coating and transform the layer of Li<sub>2</sub>S into Li<sub>x</sub>S<sub>y</sub>O (e.g., Li<sub>2</sub>SO<sub>3</sub> and Li<sub>2</sub>SO<sub>4</sub>) ([Fig. 1d](#)). The formation of Li<sub>x</sub>S<sub>y</sub>O was confirmed by our analyses using X-ray photoelectron spectroscopy (XPS), and this conversion from Li<sub>2</sub>S to Li<sub>x</sub>S<sub>y</sub>O would have some extra beneficial effects: (i) mitigate electrolyte oxidation and (ii) reduce electrode corrosion. In addition, the resultant Li<sub>x</sub>S<sub>y</sub>O coating continued to protect the NMC811 electrode in multiple aspects: (i) improving the mechanical integrity of

both the NMC powders and electrodes; (ii) stabilizing the interface between the NMC electrode and its electrolyte; and (iii) mitigating the irreversible structural phase transition of NMC materials. Consequently, this work is significant, for it may open a corner of a large area of surface coatings, in which sulfides have not been well investigated previously.

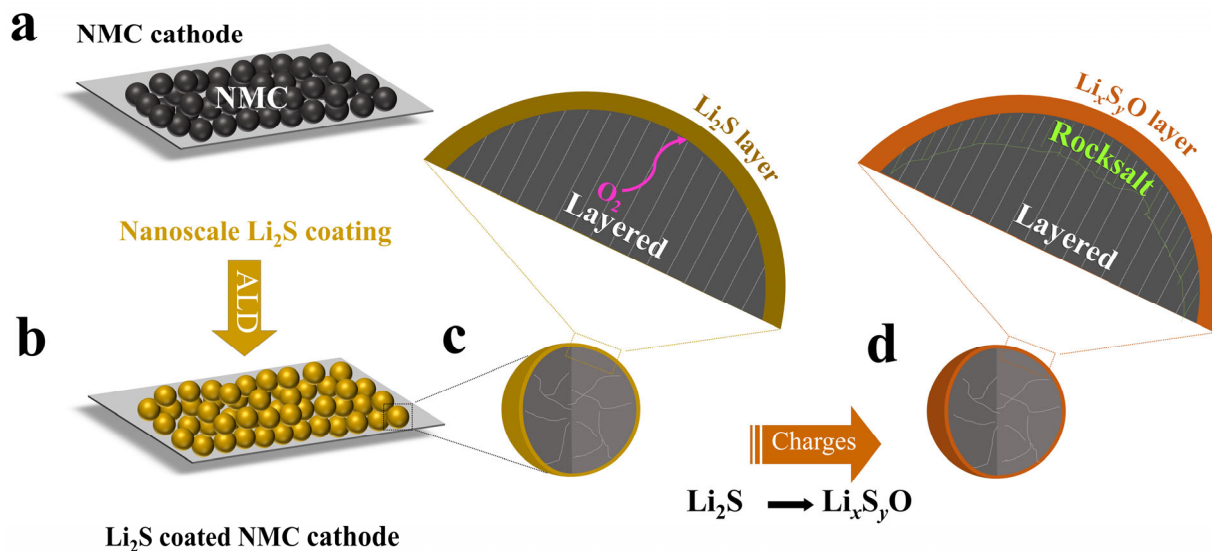


**Fig. 1.** Schematic diagram of the conversion and protection mechanism of the  $\text{Li}_2\text{S}$  ALD coating on NMC811 cathodes.

## 2. Experimental

### 2.1. Electrode preparation

The NMC811 electrode laminates in this study contain 86 wt% NMC811 powder (MSE Supplies), 7 wt% polyvinylidene fluoride (PVDF, HSV900, MTI Corporation), 7 wt% carbon black (Timical Super C65). To fabricate the laminates, a slurry was first prepared by mixing NMC811 powders, PVDF, and carbon black with a suitable amount of 1-methyl-2-pyrrolidinone (NMP, 99.5%, Sigma-Aldrich) homogeneously using a mixer (THINKY, AR-100). Then, the slurry was cast on

Al foils. The resultant NMC laminates were first vaporized completely in air and further dried in vacuum at 100 °C for 10 h. The mass loading of the prepared NMC811 is  $\sim 7.0 \text{ mg cm}^{-2}$ .

## 2.2. $\text{Li}_2\text{S}$ ALD coatings

The  $\text{Li}_2\text{S}$  ALD process has been developed in one of our previous studies [38]. In this work, the ALD- $\text{Li}_2\text{S}$  coating was deposited on prefabricated NMC811 laminates at 150 °C. The ALD system (Savannah 200, Cambridge Nanotech Inc., USA) was integrated with an Ar-filled glove box. This integrated ALD-glove box facility guaranteed no air-exposure to the  $\text{Li}_2\text{S}$ -coated NMC811 laminates during the process from the ALD deposition to the cell assembly. The  $\text{Li}_2\text{S}$  ALD was proceeded using lithium *tert*-butoxide ( $\text{LiO}^t\text{Bu}$  or LTB, 98 at%, Strem Chemicals, Inc.) and hydrogen sulfide (4 at%  $\text{H}_2\text{S}$  balanced by Ar, Airgas) as precursors. The Ar gas of ultra high purity (Airgas) was used as the carrier gas of the ALD precursors. To produce a sufficient vapor, the solid LTB was heated to 150 °C in a stainless steel bubbler. A single cycle of the  $\text{Li}_2\text{S}$  ALD was consisted of four successive steps: (1) a 3.0 s dose of LTB; (2) a 10.0 s purge using Ar gas to remove excessive LTB and byproducts; (3) a 0.5 s dose of  $\text{H}_2\text{S}$ , and (4) a 10.0 s purge using Ar gas to remove excessive  $\text{H}_2\text{S}$  and byproducts. NMC electrodes were conformally coated with  $\text{Li}_2\text{S}$  films of different thicknesses through operating ALD for 10, 20, and 40 cycles. The growth per cycle (GPC) of the ALD  $\text{Li}_2\text{S}$  was  $\sim 1.1 \text{ \AA cycle}^{-1}$ . Thus, the coating thickness was  $\sim 1, 2, \text{ and } 4 \text{ nm}$ , respectively. To discriminate these  $\text{Li}_2\text{S}$ -coated NMC electrodes, we named them as ALD-10, ALD-20, and ALD-40, respectively. Accordingly, the bare (uncoated) NMC811 electrode was signified as ALD-0.

In addition, we also deposited the  $\text{Li}_2\text{S}$  films on Si wafers for 200 ALD cycles to investigate their sensitivity to  $\text{O}_2$  and/or  $\text{H}_2\text{O}$  at room temperature. We used XPS to analyze these  $\text{Li}_2\text{S}$  films after 30-min exposures to  $\text{O}_2$  and/or  $\text{H}_2\text{O}$ .

### *2.3. Molecular layer deposition (MLD) of aluminum (Al)-based glycerol coating*

MLD, a technique analogous to ALD, is specially for growing polymeric films [39, 40]. Using trimethylaluminum (TMA) and glycerol (GL) as MLD precursors, we deposited a layer of AlGL film (200 MLD cycles, ~25 nm) over Li<sub>2</sub>S-coated Si wafers (both exposed and non-exposed) as the capping layer. The AlGL MLD process was performed at 150 °C. The AlGL capping layer could protect the Li<sub>2</sub>S-coated samples from exposure to air and thereby facilitate us to install these samples on XPS for analyses. The AlGL deposition process was performed with four steps: (1) a 0.05 s dose of TMA, (2) a 60 s purge of Ar gas to remove excessive TMA and by-products, (3) a 2 s dose of GL, and (4) a 60 s purge of Ar gas to remove excessive GL and by-products.

### *2.4. Materials characterization*

NMC811 electrodes were observed for their morphological characteristics and determined for element distribution, using a scanning electron microscopy (SEM, XL30, Philips FEI) equipped with an energy dispersive X-ray spectroscopy (EDS) at Arkansas Nano & Bio Materials Characterization Facility at the University of Arkansas (Fayetteville, AR, USA). The morphological evolution of NMC powders at the mesoscale (30 nm) also was characterized using synchrotron-based transmission X-ray microscopy (TXM) at National Synchrotron Light Source II (NSLS-II) at Brookhaven National Laboratory (BNL, NY, USA).

Transmission electron microscopy (TEM) was used to analyze NMC811 powders at Center for Nanoscale Materials (CNM) at Argonne National Laboratory (ANL, IL, USA). TEM specimens were prepared from bare and cycled NMC811 electrodes using a focused ion beam (FIB) (Zeiss NVision 40) through standard lift-out process. The elemental distribution was mapped using a scanning TEM (STEM, FEI Talos F200X) equipped with a SuperX EDS detector. The high-

resolution TEM (HR-TEM) experiment was performed on Argonne chromatic aberration-corrected TEM (ACAT) operated at 200 kV, an FEI Titan 80-300 ST equipped with a CEOS Cc/Cs image corrector to correct both spherical and chromatic aberrations at CNM at ANL. Synchrotron-based X-ray diffraction (XRD) was conducted at the beamline 11 ID-C of the Advanced Photon Source (APS) at ANL, having an X-ray wavelength of 0.1173 Å.

The Raman measurements were carried out on a Renishaw inVia Raman microscope that is a confocal micro-Raman system. The measurements were conducted on the ALD-20 electrode at CNM at ANL. Samples were sealed in a quartz container to avoid any exposure to air. Raman excitation was applied with a 532 nm laser. The spectrum was scanned with a 1200 line/mm grating. Data was recorded using a 50 × focusing/collection optic with 0.5 numerical aperture (Leica). The evolutions of surface elements of NMC811 electrodes and Li<sub>2</sub>S-coated Si wafers were analyzed using an XPS (Versa Probe III) with mono Al K<sub>α</sub> as the X-ray source (1486.6 eV) at Arkansas Nano & Bio Materials Characterization Facility at the University of Arkansas (Fayetteville, AR, USA), and the ALGL layer was removed using Ar<sup>+</sup> sputtering.

### *2.5. Electrochemical measurements*

Coin cells were assembled in an Ar-filled glove box integrated with the ALD system after NMC811 laminates were coated with the ALD Li<sub>2</sub>S films. In the glove box, O<sub>2</sub> and H<sub>2</sub>O were controlled at less than 0.01 ppm. Li metal and Celgard 2325 membrane were used as the anode and the separator, respectively. The electrolyte is 1.2 M LiPF<sub>6</sub> in ethylene carbonate (EC)/ethylmethyl carbonate (EMC) (3:7 by weight, Panax Etec Co.). All the assembled cells were rested for 10 h prior to their electrochemical tests at room temperature. Galvanostatic charge-discharge was carried out using a Neware battery test system. Different cells were tested for rate capability under various C-rates (1 C = 200 mA g<sup>-1</sup>) and cycled at 1 C for long-term cyclability

via a constant current (CC) mode in the voltage ranges of 3.0–4.3/4.5/4.7 V versus Li/Li<sup>+</sup>. Cell impedance measurements were carried out in the frequency range of 100 kHz to 10 mHz with an amplitude voltage of 5 mV using an electrochemical impedance spectroscopy (EIS, SP-200 BioLogic, USA).

### 3. Results and discussion

Fig. 2(a) illustrates the morphologies of the uncoated and Li<sub>2</sub>S-coated NMC811 electrodes. Compared with the uncoated NMC811 electrode (ALD-0) (Fig. 2a), the Li<sub>2</sub>S-coated NMC811 electrodes (i.e., ALD-10, ALD-20, and ALD-40) did not exhibit any evident changes, owing to the thin (< 5 nm) and conformal nature of the ALD Li<sub>2</sub>S coatings. The GPC of the Li<sub>2</sub>S ALD is verified being ~1.1 Å cycle<sup>-1</sup> (Fig. S1). In this regard, the elemental mapping of the ALD-20 electrode in Fig. 2(b) confirms that Ni, Mn, Co, and S are distributed uniformly. The XRD patterns of the uncoated and Li<sub>2</sub>S-coated NMC electrodes are shown in Fig. S2. All the typical XRD peaks of NMC811 are indexed for the ALD-0 and ALD-20 electrodes, indicating a layered α-NaFeO<sub>2</sub> structure in these electrodes. Furthermore, the distinct splitting of (006)/(102) peaks and (108)/(110) peaks demonstrate a well-developed layered structure. The results indicate that the ALD coatings do not cause structural changes of NMC811. In addition, there had no Li<sub>2</sub>S peaks detected, due to the amorphous nature of the ALD-deposited Li<sub>2</sub>S films [38]. Using Raman spectroscopy, we measured the ALD-20 electrode and revealed that that there had Li<sub>2</sub>S deposited on the ALD-20 electrode (Fig. S3). Combining the data of XRD and Raman, we can conclude that the deposited Li<sub>2</sub>S is amorphous. This is consistent to our previous study [38], in which Li<sub>2</sub>S films were first developed via ALD and remained being amorphous in the temperature range of 100 – 300 °C.

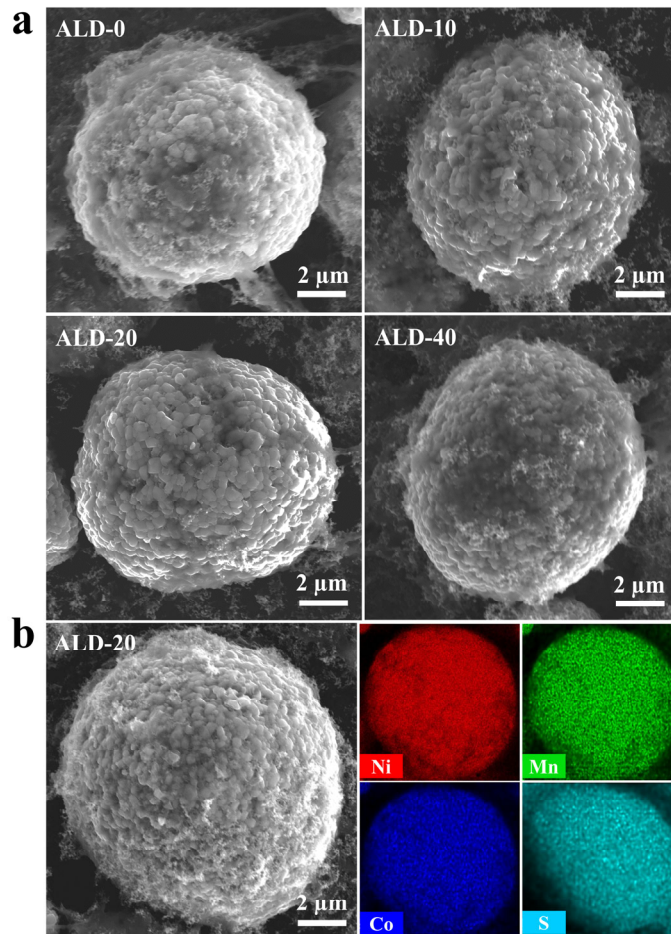


**Fig. 2.** NMC811 electrodes characterized using SEM and EDS. (a) SEM images of uncoated and Li<sub>2</sub>S-coated NMC electrodes and (b) the elemental mapping of the ALD-20 electrode by EDS.

Encouragingly, electrochemical testing revealed that the nanoscale Li<sub>2</sub>S coatings enabled improved performance. Fig. 3a(i–iii) show the rate capability of the uncoated and Li<sub>2</sub>S-coated NMC cathodes in three voltage windows of 3.0–4.3/4.5/4.7 V, respectively. These electrodes were first charged/discharged at 0.1 C for 3 cycles. Subsequently, they were charged/discharged for 5 cycles at 0.2, 0.5, 1, 2, 3, 5 and 7 C, respectively. Then, they were further tested at 0.5 C for 42 cycles. In all these three voltage windows, the rate capabilities of the uncoated and coated NMC electrodes were comparable at C-rates of  $\leq 2$  C, implying that the Li<sub>2</sub>S coating layers did not show

evident effects on the  $\text{Li}^+$  diffusion at low current densities. However, the effects of the ALD  $\text{Li}_2\text{S}$  coatings became more and more evident with increased C-rates from 3 to 5 and 7 C. The higher the C-rates, the larger the improvement of the capacities of the coated NMC811 electrodes. Among these  $\text{Li}_2\text{S}$ -coated electrodes, the ALD-20 electrode showed the best rate capability in all the cases. These results implied that there must have a trade-off between the benefits and the downsides of the  $\text{Li}_2\text{S}$  coatings. They competed for dominance over the NMC performance. Thus, there is an optimal coating thickness to maximize the positive effects of the  $\text{Li}_2\text{S}$  coatings, i.e., the ALD-20, in this study. Compared to the ALD-20, specifically, the ALD-10 might not have achieved a sufficient coating thickness to protect NMC811 electrodes while the ALD-40 might be too thick and have impeded the diffusion of  $\text{Li}^+$  considerably.

In the range of 3.0–4.3 V at 7 C (Fig. 3a(i)), the ALD-20 electrode has enabled a capacity of 76  $\text{mAh g}^{-1}$ , two times higher than the capacity of 35  $\text{mAh g}^{-1}$  of the ALD-0 electrode. Both the ALD-10 and ALD-40 have achieved a comparable capacity of 58  $\text{mAh g}^{-1}$ . In the range of 3.0–4.5 V at 7 C (Fig. 3a(ii)), the ALD-20 electrode has achieved a capacity of 92  $\text{mAh g}^{-1}$ , more than twice the capacity of 42  $\text{mAh g}^{-1}$  of the ALD-0 electrode. The ALD-10 and ALD-40 have realized a comparable capacity of 80 and 78  $\text{mAh g}^{-1}$ , respectively. In the range of 3.0–4.7 V at 7 C (Fig. 3a(iii)), the ALD-20 electrode has reached a capacity of 98  $\text{mAh g}^{-1}$ , more than two times higher than the capacity of 43  $\text{mAh g}^{-1}$  of the ALD-0 electrode. The ALD-10 and ALD-40 have enabled a capacity of 90 and 83  $\text{mAh g}^{-1}$ , respectively. These results are intriguing and have clearly demonstrated that the ALD  $\text{Li}_2\text{S}$  coatings are effective to improve the rate capabilities of NMC811 electrodes. In addition, in these three voltage ranges, all the coated and uncoated electrodes could almost recover their capacities when they were returned to test at 0.5 C. This implies that these

electrodes themselves did not change remarkably but their interfaces varied and had considerable impacts on their rate capabilities.

Additionally, we further comparatively investigated the long-term cyclability of the ALD-20 and ALD-0 electrodes in the voltage range of 3.0–4.3 V. These two electrodes were first tested at 0.1 C for 3 cycles and then they were charged at 0.5 C and discharged at 1 C for 500 cycles. The lower charging rate (i.e., 0.5 C) was to minimize the adverse influence of Li anodes, for higher charging rates are prone to cause more severe corrosion of Li metal anodes [41]. After the first 3 cycles at 0.1 C, the ALD-0 and ALD-20 electrodes had comparable capacities of  $\sim 170 \text{ mAh g}^{-1}$ . During the following 500 cycles, the ALD-20 electrode showed much better performance than that of the ALD-0 electrode (Fig. 3b). Specifically, the ALD-20 could sustain a capacity of  $122 \text{ mAh g}^{-1}$  after 500 cycles, accounting for a capacity retention of 71.3%. In contrast, the ALD-0 only retained a capacity of  $20 \text{ mAh g}^{-1}$  after 500 cycles, having a capacity retention of  $\sim 11.6\%$ . These results again have demonstrated that the ALD- $\text{Li}_2\text{S}$  coatings could dramatically improve the electrochemical performance of NMC811 electrodes. Moreover, the ALD-20 exhibited a nearly constant Coulombic efficiency (CE) of  $\sim 98\%$  while the ALD-0 could not sustain a stable CE after  $\sim 240$  cycles (Fig. 3b), corresponding to their cycling performances. We have further verified that these results were highly repeatable (see Fig. S4). Furthermore, the cyclability of ALD-0 and ALD-20 in the ranges of 3.0–4.5 and 3.0–4.7 V also was investigated and included in Fig. S5. In 200 cycles, the capacity retention of the ALD-20 electrodes was 73.5% versus 49.5% of the ALD-0 in the range of 3.0–4.5 V and 68.6% versus 47.3% of the ALD-0 in the range of 3.0–4.7 V. All these results jointly demonstrated that the 2-nm  $\text{Li}_2\text{S}$  coating could remarkably help improve the performance of the ALD-20 electrodes.

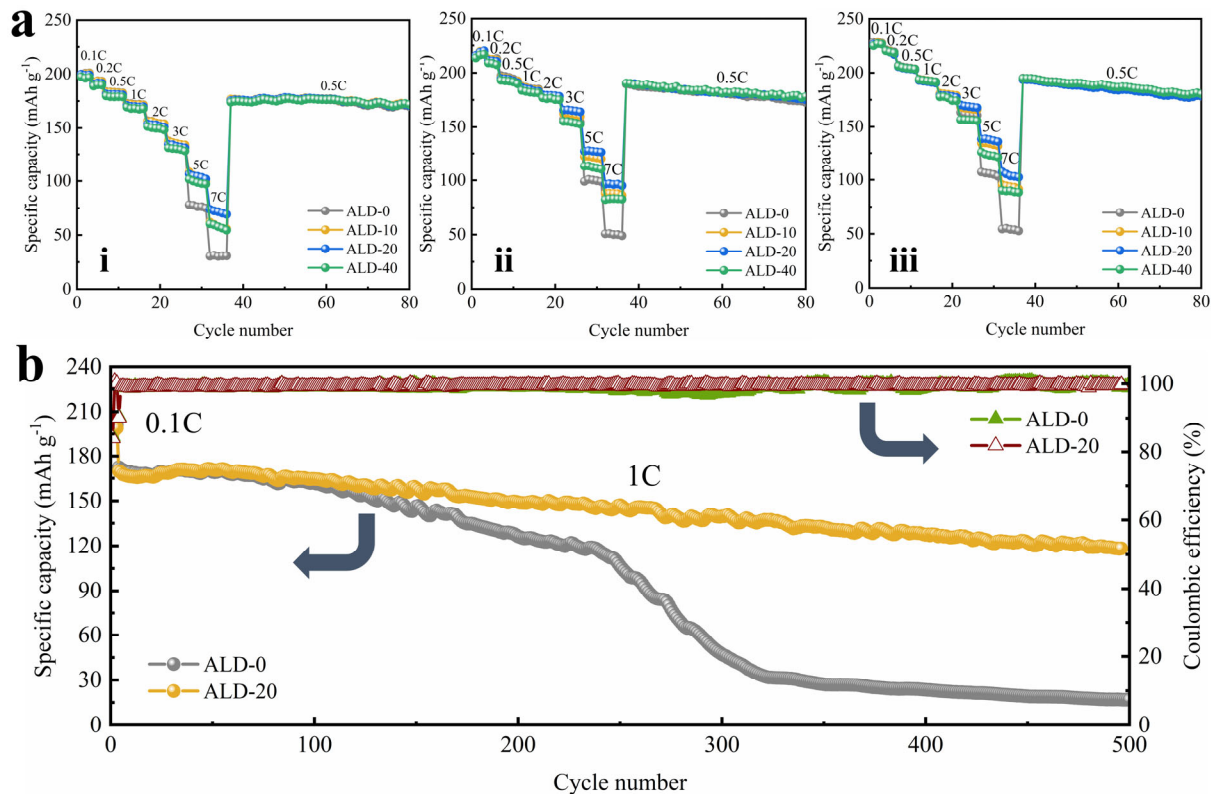


**Fig. 3. Electrochemical performance of uncoated and  $\text{Li}_2\text{S}$ -coated NMC811 electrodes.** (a) Rate capability of the uncoated and  $\text{Li}_2\text{S}$ -coated NMC811 electrodes at various current densities in a voltage range of (i) 3.0–4.3 V, (ii) 3.0–4.5 V, and (iii) 3.0–4.7 V. (b) Long-term cyclability (charge at 0.5 C and discharge at 1 C) and CE of the ALD-0 and ALD-20 electrodes in the voltage range of 3.0–4.3 V.

The beneficial effects of the ALD- $\text{Li}_2\text{S}$  coatings were further observed on sustaining the structural stability of NMC811. In this regard, we comparatively analyzed the charge-discharge profiles of the ALD-0 and ALD-20 electrodes in the range of 3.0–4.3 V, as illustrated in Fig. 4(a and b), respectively. We observed that, along with a faster capacity fading, the ALD-0 electrode also has experienced a larger voltage drop than that of the ALD-20 electrode. Fig. 4(c) illustrates the evolution of the average discharge voltage with cycles. The average discharge voltage was calculated through dividing discharge energy by discharge capacity, while the discharge energy

was obtained by integrating the area under the discharge curves [42, 43]. These two electrodes have comparable discharge voltages during their initial cycles. The average discharge voltages of the ALD-0 and ALD-20 electrodes dropped from 3.78 V commonly to 3.39 and 3.6 V, respectively. In other words, the ALD-20 electrode had a much smaller voltage drop of 0.18 V versus a voltage drop of 0.39 V of the ALD-0 electrode. The discharge voltage drop implies some irreversible phase transition from the layered structure to the spinel and/or rocksalt phase [44-46]. Thus, we concluded that the ALD-Li<sub>2</sub>S coating should have greatly mitigated the irreversible phase transition. In this regard, we further analyzed the differential capacity versus voltage ( $dQ/dV$ ), as illustrated in Fig. 4(d and e) for ALD-0 and ALD-20, respectively. One is easy to observe that the ALD-0 showed much larger shifts of their oxidation and reduction peaks than those of the ALD-20 electrode in 500 cycles. These  $dQ/dV$  results clearly indicate that the ALD-0 electrode has a larger polarization increasing with cycles, which could be caused by ever-aggravated cracking, deteriorated interfaces, or/and irreversible phase transitions. The evolutions of the  $dQ/dV$  profiles again demonstrate that the ALD-0 electrode (Fig. 4d) has a larger discharge voltage decline than that of the ALD-20 one (Fig. 4e). This corroborates that the ALD-0 suffered from more severe structural changes while the Li<sub>2</sub>S coating improved the structural stability of the ALD-20 electrode.

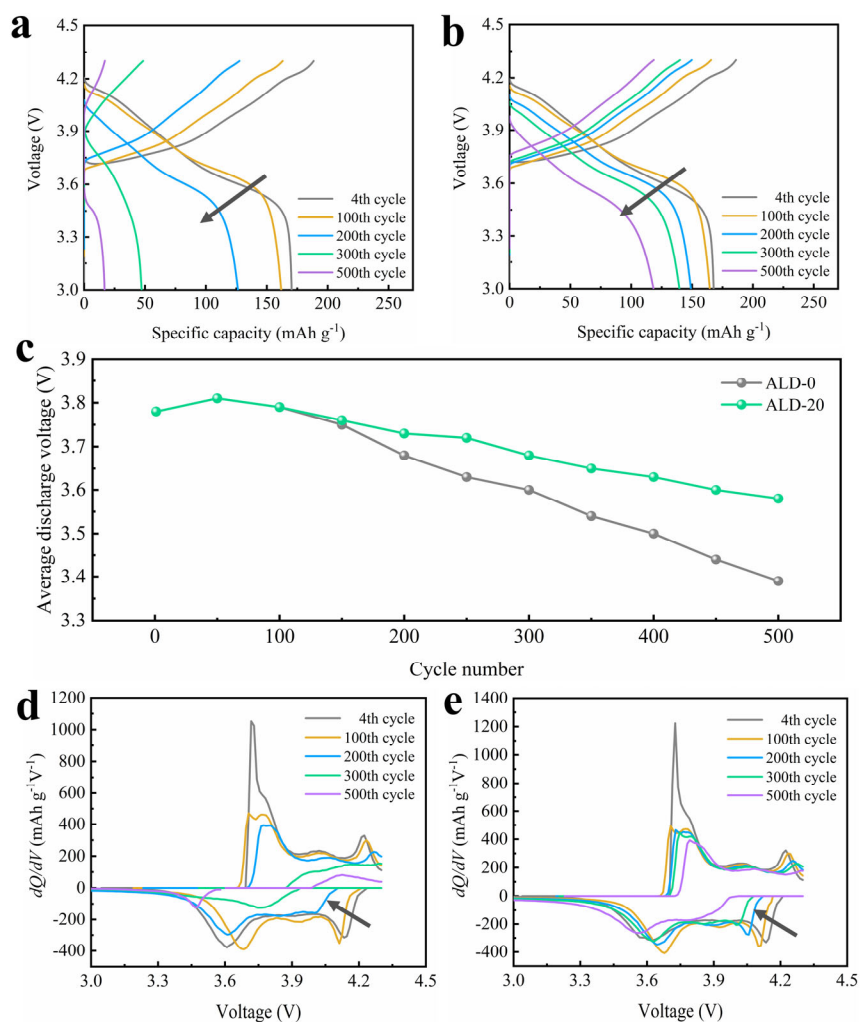


**Fig. 4. Evolutions of uncoated and  $\text{Li}_2\text{S}$ -coated NMC811 electrodes in their charge-discharge profiles and differential capacity profiles.** (a and b) Charge-discharge profiles (charge at 0.5 C and discharge at 1 C) of (a) the ALD-0 and (b) ALD-20 in the voltage range of 3.0–4.3 V. (c) Discharge voltage decay of the ALD-0 and ALD-20 electrodes at 1 C in the voltage range of 3.0–4.3 V. (d and e)  $dQ/dV$  profiles (charge at 0.5 C and discharge at 1 C) of (d) the ALD-0 and (e) the ALD-20 the voltage range of 3.0–4.3 V.

To verify our postulations on structural changes of NMC811, we observed the cycled ALD-0 and ALD-20 electrodes using SEM, as illustrated in Fig. 5(a) and Fig. S6. Apparently, many microsized secondary particles of the ALD-0 electrode have broken after 500 charge-discharge cycles (as circled by the yellow dashed line in Fig. 5a) while those of the ALD-20 have not been

observed with any evident changes in their morphology. These results indicated that the 2-nm  $\text{Li}_2\text{S}$  coating layer has remarkably strengthened the mechanical integrity of the NMC secondary particles. This partially explained the excellent capacity retention of the ALD-20 in Fig. 3(b). We further investigated the structural evolutions of the NMC powders from the cycled ALD-0 and ALD-20 electrode using synchrotron-based TXM technique. Fig. 5(b) shows the internal structure of two secondary particles from the cycled ALD-0 and ALD-20 electrodes. The corresponding cyclability is shown in Fig. S7. One can observe that the NMC811 secondary particles from the cycled ALD-0 electrode have generated numerous large cracks and their hierarchical structures have been nearly destroyed. In contrast, the secondary particles from the cycled ALD-20 electrode were nearly intact and their hierarchical structures were maintained well. Only some tiny cracks were seen from the secondary particles of the cycled ALD-20 electrode. These TXM results further confirmed that the  $\text{Li}_2\text{S}$  coating has evidently mitigated the cracking behavior of the NMC particles. This is significant, for cracks could generate more new surfaces exposed to the electrolyte, expedite oxygen release with an increased amount from NMC lattices, and therefore cause more severe side reactions at the interface of NMC811. These detrimental effects would further aggravate irreversible phase transition, cause more severe decomposition of the electrolyte, thicken the SEI layer, increase cell impedance, and eventually worsen the cell performance. All these should have underlain the more severe polarization of ALD-0 electrode in Fig. 4(d).

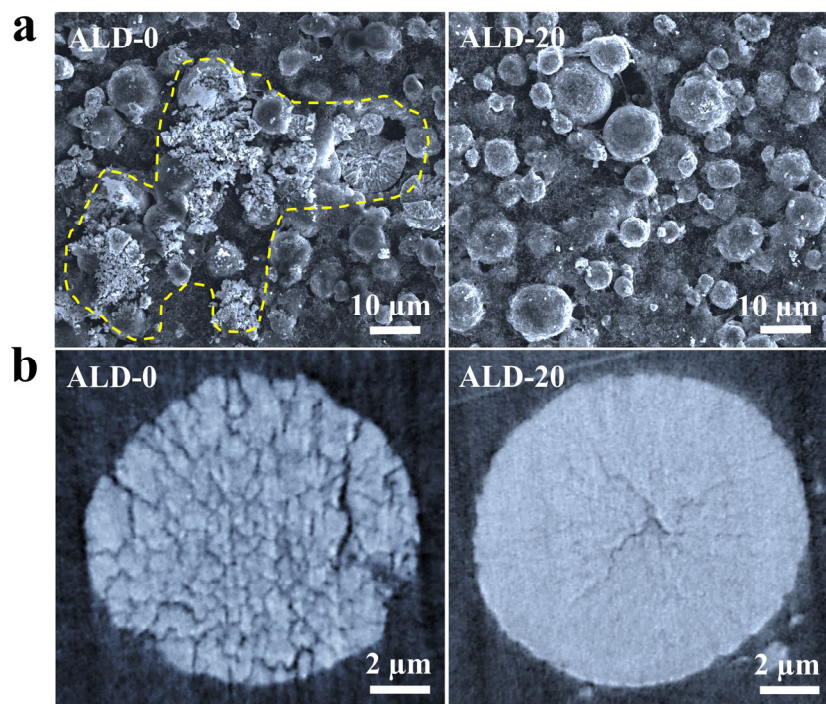


**Fig. 5. Morphological evolutions of uncoated and  $\text{Li}_2\text{S}$ -coated NMC811 electrodes.** (a) SEM images of the ALD-0 and ALD-20 electrodes after 500 charge-discharge cycles (charge at 0.5 C and discharge at 1 C) in the voltage range of 3.0–4.3 V. (b) TXM images of NMC powders from the ALD-0 and ALD-20 electrodes after 200 charge-discharge cycles (charge at 0.5 C and discharge at 3 C) in the voltage range of 3.0–4.5 V.

To further characterize the morphological and structural evolutions of the uncoated (ALD-0) and  $\text{Li}_2\text{S}$ -coated (ALD-20) electrodes after 500 charge-discharge cycles, we employed a suite of electron microscopies. In the case of the ALD-0 electrode, the FIB-SEM image of the cross section of one cycled secondary NMC811 particle clearly showed that there were numerous cracks produced from the surface to the central area of the particle (Fig. 6a). HR-TEM analyses on a local area (as circled by the yellow dashed line in Fig. 6a) further revealed that cracks exposed more particles to the electrolyte and thereby the local particle surface was covered by a thick SEI layer. The thickness of SEI layers varied with locations and could reach up to 10 nm or higher (Fig. 6b and Fig. S8b-d). HR-TEM also disclosed that the local particle surface has experienced serious

phase transition irreversibly from its initial layered structure (see Figure S8a) to the NiO-like rocksalt structure (Fig. 6b). This irreversible phase change has been witnessed by the (003) planes of the layered structure (having the 0.47-nm lattice spacing) [47] and the (111) planes of NiO-like structure (having the 0.24-nm lattice spacing) [48] (Fig. 6b). Particularly, the rocksalt layer could reach up to 20 nm thick. More HR-TEM images of the local area are included in Figure S8(b).

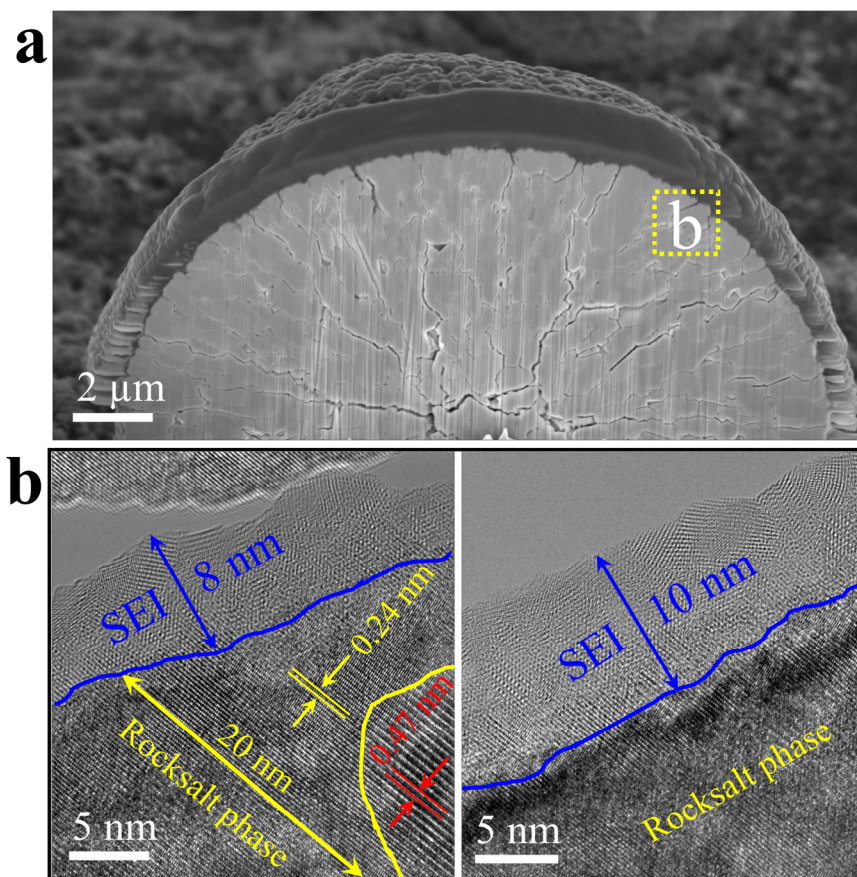


**Fig. 6. Characterizations of the cycled bare NMC811 using electron microscopies.** (a) FIB-SEM and (b) HR-TEM images of the cycled ALD-0 electrode after 500 charge-discharge cycles (charged at 0.5 C and discharged at 1.0 C) in the voltage range of 3.0 – 4.3 V.

In the case of the cycled ALD-20 electrode, we employed STEM and HR-TEM to analyze its morphological and structural evolutions. We conducted TEM elemental mapping on the selected

area “I” (as marked by the yellow dashed line in Fig. 7a(i)) of a local area of a cycled Li<sub>2</sub>S-coated NMC811 particle. As shown in Fig. 7a(ii–iv), the STEM-EDS mapping images revealed some TMs on the surface of the NMC particle from the cycled ALD-20 electrode. It implies that the 2-nm Li<sub>2</sub>S coating must have mitigated the issue of the dissolution of TMs but the coating has degraded after 500 charge-discharge cycles. Ni has the strongest mapping signal on the surface, due to the highest content of Ni in NMC811. Fig. 7a(v and vi) show the distribution of both O and S on the surfaces of NMC particles, implying a potential conversion from the Li<sub>2</sub>S coating layer to a Li<sub>x</sub>S<sub>y</sub>O coating layer. The non-conformal S distribution in Fig. 7a(vi) implies that the Li<sub>2</sub>S coating layer must have degraded after 500 charge-discharge cycles. This degradation of the Li<sub>2</sub>S coating could occur in two aspects: (i) the long-term mechanical impacts might have led to some local failures and (ii) the Li<sub>2</sub>S coating layer might have reacted with some active oxygen released from the phase transitions of NMC to produce sulfates (e.g., Li<sub>x</sub>S<sub>y</sub>O). To this end, we employed HR-TEM to observe the surface structures of the cycled NMC811 particles of the ALD-20 electrode (Fig. 7b). Some minor microcracks could be observed from the bulk structure of the ALD-20 electrode in Fig. 7b(i), which have also been seen in the above TXM images in Fig. 5. To further analyze, the selected area “II” of Fig. 7b(i) is further shown in Fig. 7b(ii) and the selected area “III” of Fig. 7b(ii) is exhibited in Fig. 7b(iii). Observing the local lattice spacings in Fig. 7b(iii), we could conclude that the NMC particles remained their layered structures in their main bodies but their surfaces have experienced some irreversible layered-rocksalt phase transition after 500 charge-discharge cycles. Impressively, the rocksalt phase layer of the NMC powders from the cycled ALD-20 electrode was only ~5 nm thick at most after 500 charge-discharge cycles, which is much less than the 20-nm thick rocksalt layer of the cycled ALD-0 electrode (Fig. 6(b)). In addition, there lacked an evident SEI layer with the cycled ALD-20 electrode. In addition to

mitigating microcracking, apparently, the nanoscale  $\text{Li}_2\text{S}$  coating has also significantly suppressed the irreversible layered-rocksalt phase transition and inhibited the SEI formation. All these were beneficial to maintain the higher performance of the ALD-20 electrode (as shown in Fig. 3).

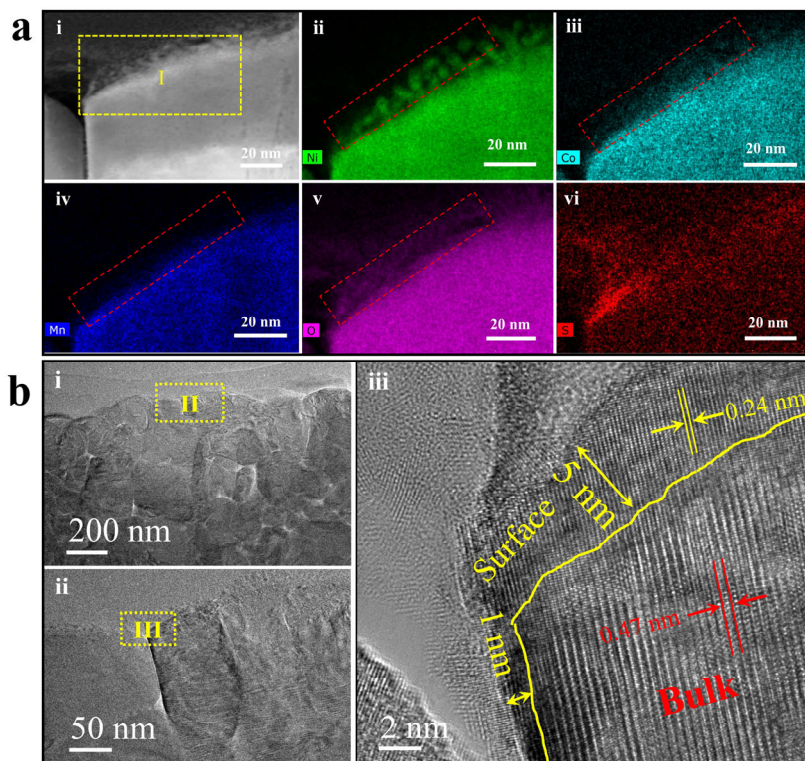


**Fig. 7. Characterizations of the cycled  $\text{Li}_2\text{S}$ -coated NMC811 particles using electron microscopies.** (a) STEM-EDS image and elemental mapping and (b) HR-TEM images of the ALD-20 electrode after 500 charge-discharge cycles at 1 C in the voltage range of 3.0–4.3 V.

To study and verify our postulation that the ALD  $\text{Li}_2\text{S}$  coating might have converted to  $\text{Li}_x\text{S}_y\text{O}$  through reacting with  $\text{O}_2$  or/and  $\text{H}_2\text{O}$  (some trace water may exist in electrolytes), we deposited  $\text{Li}_2\text{S}$  films over Si wafers and then exposed  $\text{Li}_2\text{S}$ -coated Si wafers to pure  $\text{O}_2$  vapor, pure  $\text{H}_2\text{O}$  vapor, and the alternative dosing of the pure  $\text{O}_2$  and  $\text{H}_2\text{O}$  vapor at room temperature for 30 min, respectively. The  $\text{Li}_2\text{S}$ -coated Si substrates with and without exposures were then capped with a protective layer of AIGL via MLD and subsequently analyzed for their S 2p and Li 1s using high-resolution XPS (Fig. 8a–d). All the peaks of S 2p at 159.4 (or 159.6), 160.9, and 162.0 eV are

assigned to  $\text{Li}_2\text{S}$  while the peak of Li 1s at 54.2 eV is also ascribed to  $\text{Li}_2\text{S}$  [49-54]. Compared to the pristine  $\text{Li}_2\text{S}$  (Fig. 8a), the  $\text{Li}_2\text{S}$  films exposed to  $\text{O}_2$  (Fig. 8b) and to both  $\text{O}_2$  and  $\text{H}_2\text{O}$  (Fig. 8d) commonly have a new peak of S 2p at 167.2 eV, which is assigned to  $\text{SO}_3^{2-}$  [55-57], i.e.,  $\text{Li}_2\text{SO}_3$ . Such a peak was not observed with the  $\text{Li}_2\text{S}$  film exposed to  $\text{H}_2\text{O}$  (Fig. 8c), implying that  $\text{SO}_3^{2-}$  originated from the oxidation of  $\text{Li}_2\text{S}$  with  $\text{O}_2$  exposure but not  $\text{H}_2\text{O}$  exposure. The existence of  $\text{Li}_2\text{SO}_3$  has further been validated by the new peak of Li 1s at 55.2 eV for the  $\text{Li}_2\text{S}$  films exposed to  $\text{O}_2$  (Fig. 8b) and to both  $\text{O}_2$  and  $\text{H}_2\text{O}$  (Fig. 8d) [58-60]. The peak at 54.3 eV is assigned to  $\text{Li}_2\text{S}$  [61]. For the  $\text{Li}_2\text{S}$  exposed to  $\text{H}_2\text{O}$  (Fig. 8c), the peaks at 55.5 and 56.5 eV are due to  $\text{LiOH}$  [62, 63] and  $\text{RCO}_3\text{Li}/\text{Li}_2\text{CO}_3$  [63, 64], respectively.  $\text{LiOH}$  should be formed via the reaction:  $\text{Li}_2\text{S} + \text{H}_2\text{O} \rightarrow \text{LiOH} + \text{H}_2\text{S}$  [65]. The formation of  $\text{RCO}_3\text{Li}/\text{Li}_2\text{CO}_3$  was not clear and might be due to the  $\text{Ar}^+$  sputter on the AlGL capping layer. To sum up, the oxygen exposure of the ALD-deposited  $\text{Li}_2\text{S}$  films could lead to the formation of  $\text{Li}_2\text{SO}_3$  (Fig. 8b) while water exposure resulted in the production of  $\text{LiOH}$  (Fig. 8c). It was not surprising that the combined oxygen and water exposure of  $\text{Li}_2\text{S}$  films contributed to the formation of both  $\text{Li}_2\text{SO}_3$  and  $\text{LiOH}$  (Fig. 8d).

We also utilized XPS to analyze the S 2p and Li 1s of the cycled ALD-20 electrode after 20 charge-discharge cycles (Fig. 8e). The peaks of S 2p at 168.6 and 169.6 eV are assigned to  $\text{Li}_2\text{SO}_3$  [66] and  $\text{Li}_2\text{SO}_4$  [57, 67], respectively. The existence of  $\text{Li}_2\text{SO}_3$  and  $\text{Li}_2\text{SO}_4$  has been further confirmed by the peaks of Li 1s at 55.2 and 56 eV [68], respectively. According to the XPS spectra of S 2p and Li 1s (Fig. 8e), apparently, there has a remarkably reduced amount of  $\text{Li}_2\text{S}$  left with the cycled ALD-20 electrode, which is evidenced by the weakened peak of S 2p at 160.4 eV [67] and the decreased peak of Li 1s at 54.2 eV. Furthermore, there has a noticeable peak of S 2p at 163.8 eV (Fig. 8e), which should be ascribed to the bond of Ni-S [69-72] but was not identifiable on the uncycled ALD-20 electrode (as shown in Fig. S3 by Raman spectra). This peak indicates that the

deposited  $\text{Li}_2\text{S}$  has partially bonded to Ni during the charge-discharge cycles. Based on the information discussed above, it is reasonable to conclude that, during the charge-discharge processes in the range of 3.0 – 4.3 V, the ALD-deposited  $\text{Li}_2\text{S}$  coating has mainly converted to  $\text{Li}_2\text{SO}_3$  and  $\text{Li}_2\text{SO}_4$ . The oxidation process of  $\text{Li}_2\text{S}$  might have proceeded from  $\text{Li}_2\text{SO}_3$  to  $\text{Li}_2\text{SO}_4$ . Such a process has been suggested in literature in other sulfur-related compounds applied in NMC cathodes [73, 74]. We will further clarify this in our future study. This conversion process itself was beneficial, for it consumed  $\text{O}_2$  released from NMC lattices, then protected the electrolyte from decomposition, and thereby avoided many subsequent detrimental effects such as the production of  $\text{CO}_2$  and  $\text{H}_2\text{O}$  [75, 76]. Furthermore, the converted  $\text{Li}_x\text{S}_y\text{O}$  coating show some more benefits: (i) strengthening the mechanical integrity of the NMC electrodes; (ii) stabilizing the NMC electrode/electrolyte interface; and (iii) suppressing the irreversible phase transition of the NMC structure. Compared to the electronically and ionically insulating nature of  $\text{Li}_2\text{S}$ , particularly,  $\text{Li}_x\text{S}_y\text{O}$  has been reported for its ionic conductivity and its rejection to electron transfer [77-80]. All these beneficial effects jointly have contributed to the improved electrochemical performance of the  $\text{Li}_2\text{S}$ -coated NMC811 electrodes. Consequently, the  $\text{Li}_2\text{S}$ -coated NMC811 cathode (e.g., ALD-20) has achieved an extended cyclability up to 500 discharge-charge cycles. In summary, this work is significant, for it might have discovered a new class of coating materials to effectively address the issues of NMCs and other electrode materials.

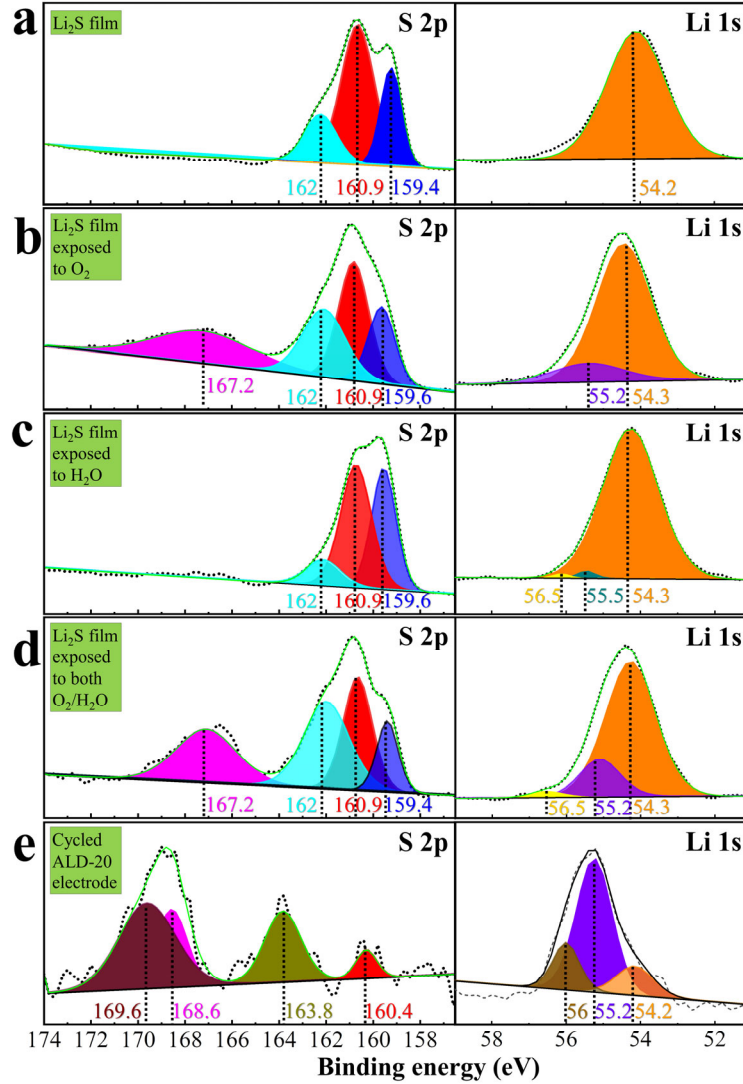


**Fig. 8. High-resolution XPS analyses of S 2p and Li 1s.** ALD-deposited Li<sub>2</sub>S films on Si wafers: (a) pristine, (b) exposed to O<sub>2</sub>, (c) exposed to H<sub>2</sub>O, and (d) exposed to both O<sub>2</sub> and H<sub>2</sub>O. The exposures were for 30 min at room temperature. (e) the ALD-20 electrode after 20 charge-discharge cycles at 1.0 C in the range of 3.0 – 4.3 V.

We also have conducted EIS measurements to clarify the effects of the ALD Li<sub>2</sub>S coating on cell impedance (Fig. 9a–c). The equivalent circuit is illustrated in Fig. 9(d). Each Nyquist plot consists of a small intercept in the real axis at high frequency region, two semicircles, and a straight line [13, 26]. The small intercept is assigned to the solution resistance ( $R_s$ ). The semicircles at high and medium frequencies represent the Li<sup>+</sup> diffusion resistance ( $R_f$ ) in the cathode surface layer, and

charge transfer resistance ( $R_{ct}$ ) at the electrode/electrolyte interface, respectively. The straight line at low frequency refers to Warburg impedance ( $W$ ), reflecting the  $\text{Li}^+$  diffusion through the solid electrode. The electrochemical resistance of ALD-0 and ALD-20 electrodes at 4.3 V vs.  $\text{Li}/\text{Li}^+$  are listed in [Table 1](#). The  $R_s$  values were almost identical and unchanged after 50 cycles for both the ALD-0 and ALD-20 but increase slightly after 100 cycles. Compared to the uncoated ALD-0 electrode, the  $R_f$  values of the  $\text{Li}_2\text{S}$ -coated electrodes were a little bit smaller after the first cycle. With some extended cycles, the  $R_f$  values of the ALD-0 electrode increased significantly from 17.66 to 33.18  $\Omega$  (i.e., increased by 88%). In contrast, the  $R_f$  values of the ALD-20 electrode only changed slightly and were much smaller (increased by 14%). This confirms that the  $\text{Li}_2\text{S}$  coating (or the converted  $\text{Li}_x\text{S}_y\text{O}$  coating) has effectively protected the NMC electrode from side reactions, undesirable structural transformation, and mechanical failure. The  $R_{ct}$  values of the ALD-20 were a little higher than those of the ALD-0 electrode. This should be due to the low ionic conductivity of the  $\text{Li}_2\text{S}$  coating layer (or the converted  $\text{Li}_x\text{S}_y\text{O}$  coating). However, the  $R_f + R_{ct}$  values of the ALD-20 electrode were remarkably smaller than those of the ALD-0 electrode after certain cycles. This is consistent to the structural evolutions of the ALD-0 and ALD-20 electrodes, as revealed in [Fig. 5-7](#). The  $R_f + R_{ct}$  values could reflect the overall resistance across the electrode/electrolyte interface. Thus, this could be one reason of the better electrochemical performance of ALD-20 than that of ALD-0.

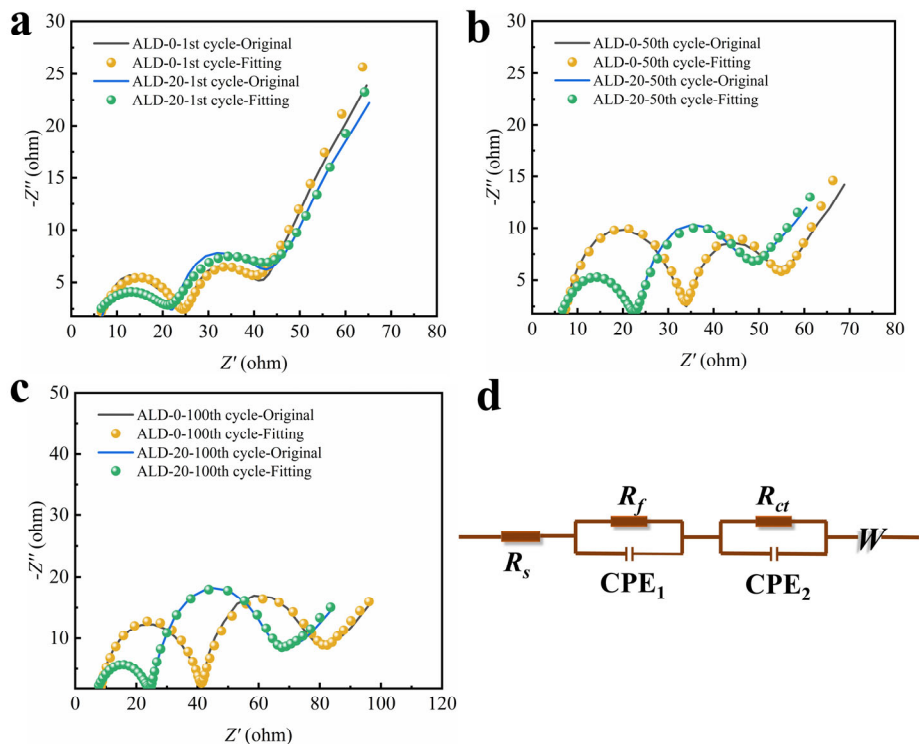


**Fig. 9.** Nyquist plots and fitting data of the ALD-0 electrode and the ALD-20 electrode with an amplitude of 5.0 mV over a frequency range of 100 kHz to 0.01 Hz: (a) the 1st cycle, (b) the 50th cycle, (c) the 100th cycle and (d) The equivalent circuit. Each cell was charged to 4.3 V at 0.5 C before the EIS measurement.

**Table 1.** Electrochemical resistance of the uncoated and Li<sub>2</sub>S-coated electrodes under an upper cutoff voltage of 4.3 V.

Cycle	Electrode	$R_s$ ( $\Omega$ )	$R_f$ ( $\Omega$ )	$R_{ct}$ ( $\Omega$ )	$R_f + R_{ct}$ ( $\Omega$ )
1st	ALD-0	6.72	17.66	17.20	34.86
	ALD-20	6.71	14.62	20.72	35.34
50th	ALD-0	6.78	27.16	21.00	48.16
	ALD-20	6.75	15.80	26.50	42.30
100th	ALD-0	7.89	33.18	40.78	73.96
	ALD-20	7.47	16.66	43.22	59.88

#### **4. Conclusions**

In this study, we made the first attempt to investigate sulfides as coating materials on NMC cathodes. We investigated the effects of the ALD  $\text{Li}_2\text{S}$  coatings on NMC811 electrodes at three different upper cutoff voltages of 4.3, 4.5, and 4.7 V. It was found that the ALD coatings dramatically improved the electrochemical performance of the NMC811 electrodes, in terms of their long cyclability, working voltage, and rate capability. Our analyses further uncovered that the ALD coatings should have beneficial effects in three aspects: (i) improve the mechanical integrity of the NMC811 electrode and NMC powders themselves; (ii) stabilize the interface between the NMC electrode and the electrolyte; (iii) mitigate the structural phase transition of NMC materials; and (iv) remove  $\text{O}_2$  released from NMC lattices. All these beneficial effects of the ALD  $\text{Li}_2\text{S}$  coatings are significant for addressing the technical issues of NMC811 electrodes and helpful for designing high-performance LIBs. This work is inspiring and very valuable for us to address the issues of NMC cathodes ultimately. It may open a corner for researchers to investigate a large variety of sulfides as new coating films for high-performance NMCs and other cathodes.

#### **Acknowledgments**

We acknowledge partial support from the Center for Advanced Surface Engineering, under the National Science Foundation Grant No. OIA-1457888 and the Arkansas EPSCoR Program, ASSET III. X.M. also appreciate the financial support from the University of Arkansas, Fayetteville, AR, USA. Research was funded by the U.S. Department of Energy (DOE), Vehicle Technologies Office. Argonne National Laboratory is operated for the U.S. Department of Energy by UChicago Argonne, LLC, under Contract DE-AC02-06CH11357. Portions of this work were performed at Advanced Photon Source (APS) and Center for Nanoscale Materials (CNM), Argonne National Laboratory. This research used resources of the Advanced Photon Source and

Center for Nanoscale Materials, Office of Science User Facility, supported by the U.S. Department of Energy, Office of Science, Office of Basic Energy Sciences, Argonne National Laboratory under Contract No. DE-AC02-06CH11357. This research used resources of the National Synchrotron Light Source II, a U.S. Department of Energy (DOE) Office of Science User Facility operated for the DOE Office of Science by Brookhaven National Laboratory under Contract No. DE-SC0012704.

### Reference:

- [1] P. Dong, D. Wang, Y. Yao, X. Li, Y. Zhang, J. Ru, T. Ren, *Journal of Power Sources*, 344 (2017) 111-118.
- [2] Z. Zheng, X.-D. Guo, S.-L. Chou, W.-B. Hua, H.-K. Liu, S.X. Dou, X.-S. Yang, *Electrochimica Acta*, 191 (2016) 401-410.
- [3] T. Li, X. Li, Z. Wang, H. Guo, *J. Power Sources*, 342 (2017) 495-503.
- [4] X. Zhang, W.J. Jiang, A. Mauger, Qilu, F. Gendron, C.M. Julien, *Journal of Power Sources*, 195 (2010) 1292-1301.
- [5] S.-M. Bak, E. Hu, Y. Zhou, X. Yu, S.D. Senanayake, S.-J. Cho, K.-B. Kim, K.Y. Chung, X.-Q. Yang, K.-W. Nam, *ACS Appl. Mater. Interfaces*, 6 (2014) 22594-22601.
- [6] R. Jung, M. Metzger, F. Maglia, C. Stinner, H.A. Gasteiger, *Journal of The Electrochemical Society*, 164 (2017) A1361-A1377.
- [7] P. Yan, J. Zheng, J. Liu, B. Wang, X. Cheng, Y. Zhang, X. Sun, C. Wang, J.-G. Zhang, *Nature Energy*, 3 (2018) 600-605.
- [8] P. Yan, J. Zheng, M. Gu, J. Xiao, J.-G. Zhang, C.-M. Wang, *Nature Communications*, 8 (2017) 14101.
- [9] H. Wang, W. Ge, W. Li, F. Wang, W. Liu, M.-Z. Qu, G. Peng, *ACS Applied Materials & Interfaces*, 8 (2016) 18439-18449.
- [10] H. Kim, M.G. Kim, H.Y. Jeong, H. Nam, J. Cho, *Nano Letters*, 15 (2015) 2111-2119.
- [11] Y. Shi, M. Zhang, D. Qian, Y.S. Meng, *Electrochimica Acta*, 203 (2016) 154-161.
- [12] J. Ahn, E.K. Jang, S. Yoon, S.-J. Lee, S.-J. Sung, D.-H. Kim, K.Y. Cho, *Applied Surface Science*, 484 (2019) 701-709.
- [13] X. Wang, J. Cai, Y. Liu, X. Han, Y. Ren, J. Li, Y. Liu, X. Meng, *Nanotechnology*, 32 (2020) 115401.
- [14] Y. Liu, X. Wang, J. Cai, X. Han, D. Geng, J. Li, X. Meng, *Journal of Materials Science & Technology*, 54 (2020) 77-86.
- [15] F. Schipper, M. Dixit, D. Kovacheva, M. Talianker, O. Haik, J. Grinblat, E.M. Erickson, C. Ghanty, D.T. Major, B. Markovsky, D. Aurbach, *Journal of Materials Chemistry A*, 4 (2016) 16073-16084.
- [16] S. Liu, Z. Dang, D. Liu, C. Zhang, T. Huang, A. Yu, *Journal of Power Sources*, 396 (2018) 288-296.

- [17] Q. Xie, W. Li, A. Manthiram, *Chem. Mater.*, 31 (2019) 938-946.
- [18] A.K. Haridas, Q.A. Nguyen, T. Terlier, R. Blaser, S.L. Biswal, *ACS Applied Materials & Interfaces*, 13 (2021) 2662-2673.
- [19] M. Hekmatfar, I. Hasa, R. Eghbal, D.V. Carvalho, A. Moretti, S. Passerini, *Advanced Materials Interfaces*, 7 (2020) 1901500.
- [20] T. Taskovic, L.M. Thompson, A. Eldesoky, M.D. Lumsden, J.R. Dahn, *Journal of The Electrochemical Society*, 168 (2021) 010514.
- [21] Y.S. Jung, A.S. Cavanagh, L.A. Riley, S.-H. Kang, A.C. Dillon, M.D. Groner, S.M. George, S.-H. Lee, *Advanced Materials*, 22 (2010) 2172-2176.
- [22] X. Meng, *Journal of Materials Research*, (2020) 1-24.
- [23] X. Meng, *Energy Storage Materials*, 30 (2020) 296-328.
- [24] X. Meng, X.-Q. Yang, X. Sun, *Advanced Materials*, 24 (2012) 3589-3615.
- [25] S.-T. Myung, K. Izumi, S. Komaba, Y.-K. Sun, H. Yashiro, N. Kumagai, *Chemistry of Materials*, 17 (2005) 3695-3704.
- [26] W. Liu, X. Li, D. Xiong, Y. Hao, J. Li, H. Kou, B. Yan, D. Li, S. Lu, A. Koo, K. Adair, X. Sun, *Nano Energy*, 44 (2018) 111-120.
- [27] Y. Chen, Y. Zhang, B. Chen, Z. Wang, C. Lu, *Journal of Power Sources*, 256 (2014) 20-27.
- [28] H. Gao, J. Cai, G.-L. Xu, L. Li, Y. Ren, X. Meng, K. Amine, Z. Chen, *Chemistry of Materials*, 31 (2019) 2723-2730.
- [29] D. Becker, M. Börner, R. Nölle, M. Diehl, S. Klein, U. Rodehorst, R. Schmuck, M. Winter, T. Placke, *ACS Applied Materials & Interfaces*, 11 (2019) 18404-18414.
- [30] F. Tao, X.-x. Yan, J.-J. Liu, H.-L. Zhang, L. Chen, *Electrochimica Acta*, 210 (2016) 548-556.
- [31] H. Liang, Z. Wang, H. Guo, J. Wang, J. Leng, *Applied Surface Science*, 423 (2017) 1045-1053.
- [32] G. Hu, Y. Tao, Y. Lu, J. Fan, L. Li, J. Xia, Y. Huang, Z. Zhang, H. Su, Y. Cao, *ChemElectroChem*, 6 (2019) 4773-4780.
- [33] Y.-D. Xu, W. Xiang, Z.-G. Wu, C.-L. Xu, Y.-C. Li, X.-D. Guo, G.-P. Lv, X. Peng, B.-H. Zhong, *Electrochimica Acta*, 268 (2018) 358-365.
- [34] Y. Liu, X. Wang, S.K. Ghosh, M. Zou, H. Zhou, X. Xiao, X. Meng, *Dalton Transactions*, (2022).
- [35] Z. Chen, G.-T. Kim, D. Bresser, T. Diemant, J. Asenbauer, S. Jeong, M. Copley, R.J. Behm, J. Lin, Z. Shen, S. Passerini, *Advanced Energy Materials*, 8 (2018) 1801573.
- [36] S. Dai, G. Yan, L. Wang, L. Luo, Y. Li, Y. Yang, H. Liu, Y. Liu, M. Yuan, *Journal of Electroanalytical Chemistry*, 847 (2019) 113197.
- [37] X. Xiong, Z. Wang, X. Yin, H. Guo, X. Li, *Materials Letters*, 110 (2013) 4-9.
- [38] X. Meng, D.J. Comstock, T.T. Fister, J.W. Elam, *ACS Nano*, 8 (2014) 10963-10972.
- [39] X. Meng, *Journal of Materials Chemistry A*, 5 (2017) 18326-18378.
- [40] X. Meng, K.C. Lau, H. Zhou, S.K. Ghosh, M. Benamara, M. Zou, *Energy Material Advances*, 2021 (2021) 9786201.
- [41] S. Jiao, J. Zheng, Q. Li, X. Li, M.H. Engelhard, R. Cao, J.-G. Zhang, W. Xu, *Joule*, 2 (2018) 110-124.
- [42] Y. Gao, R.L. Patel, K.-Y. Shen, X. Wang, R.L. Axelbaum, X. Liang, *ACS Omega*, 3 (2018) 906-916.
- [43] Y. Gao, Z. Shang, X. He, T. White, J. Park, X. Liang, *Electrochim. Acta*, 318 (2019) 513-524.
- [44] M. Bettge, Y. Li, K. Gallagher, Y. Zhu, Q. Wu, W. Lu, I. Bloom, D.P. Abraham, *Journal of The Electrochemical Society*, 160 (2013) A2046-A2055.

- [45] D. Mohanty, S. Kalnaus, R.A. Meisner, K.J. Rhodes, J. Li, E.A. Payzant, D.L. Wood, C. Daniel, *Journal of Power Sources*, 229 (2013) 239-248.
- [46] A. Boulineau, L. Simonin, J.-F. Colin, C. Bourbon, S. Patoux, *Nano Lett.*, 13 (2013) 3857-3863.
- [47] T. Deng, X. Fan, L. Cao, J. Chen, S. Hou, X. Ji, L. Chen, S. Li, X. Zhou, E. Hu, D. Su, X.-Q. Yang, C. Wang, *Joule*, 3 (2019) 2550-2564.
- [48] Y. Zhang, T. Ji, W. Zhang, G. Guan, Q. Ren, K. Xu, X. Huang, R. Zou, J. Hu, *J. Mater. Chem. C*, 5 (2017) 12520-12528.
- [49] K. Han, J. Shen, C.M. Hayner, H. Ye, M.C. Kung, H.H. Kung, *Journal of Power Sources*, 251 (2014) 331-337.
- [50] Y. Zhan, H. Yu, L. Ben, Y. Chen, X. Huang, *Electrochimica Acta*, 255 (2017) 212-219.
- [51] R. Demir-Cakan, M. Morcrette, Gangulibabu, A. Guéguen, R. Dedryvère, J.-M. Tarascon, *Energy & Environmental Science*, 6 (2013) 176-182.
- [52] G. Ai, Q. Hu, L. Zhang, K. Dai, J. Wang, Z. Xu, Y. Huang, B. Zhang, D. Li, T. Zhang, G. Liu, W. Mao, *ACS Applied Materials & Interfaces*, 11 (2019) 33987-33999.
- [53] X.-B. Cheng, C. Yan, X. Chen, C. Guan, J.-Q. Huang, H.-J. Peng, R. Zhang, S.-T. Yang, Q. Zhang, *Chem*, 2 (2017) 258-270.
- [54] C.-P. Yang, Y.-X. Yin, Y.-G. Guo, L.-J. Wan, *Journal of the American Chemical Society*, 137 (2015) 2215-2218.
- [55] H. Chu, H. Noh, Y.-J. Kim, S. Yuk, J.-H. Lee, J. Lee, H. Kwack, Y. Kim, D.-K. Yang, H.-T. Kim, *Nature Communications*, 10 (2019) 188.
- [56] V. Shutthanandan, M. Nandasiri, J. Zheng, M.H. Engelhard, W. Xu, S. Thevuthasan, V. Murugesan, *Journal of Electron Spectroscopy and Related Phenomena*, 231 (2019) 2-10.
- [57] M.J. Lacey, A. Yalamanchili, J. Maibach, C. Tengstedt, K. Edström, D. Brandell, *RSC Advances*, 6 (2016) 3632-3641.
- [58] S. Eijima, H. Sonoki, M. Matsumoto, S. Taminato, D. Mori, N. Imanishi, *J. Electrochem. Soc.*, 166 (2019) A5421-A5429.
- [59] H. Xu, P.-H. Chien, J. Shi, Y. Li, N. Wu, Y. Liu, Y.-Y. Hu, J.B. Goodenough, *Proceedings of the National Academy of Sciences*, 116 (2019) 18815.
- [60] D. Aurbach, E. Pollak, R. Elazari, G. Salitra, C.S. Kelley, J. Affinito, *Journal of The Electrochemical Society*, 156 (2009) A694.
- [61] Z.W. Seh, H. Wang, N. Liu, G. Zheng, W. Li, H. Yao, Y. Cui, *Chemical Science*, 5 (2014) 1396-1400.
- [62] L.M. Riegger, R. Schlem, J. Sann, W.G. Zeier, J. Janek, *Angewandte Chemie International Edition*, 60 (2021) 6718-6723.
- [63] Y. Wu, T. Okajima, T. Ohsaka, *Int. J. Electrochem. Sci*, 12 (2017) 1004-1013.
- [64] J. Zhang, H. Yu, X. Zhang, M. Xia, X. Zhang, L. Zhang, M. Shui, Y. Cui, *J. Shu, Ionics*, 27 (2021) 31-37.
- [65] F. Wan, L. Fang, X. Zhang, C.A. Wolden, Y. Yang, *Journal of Energy Chemistry*, 63 (2021) 138-169.
- [66] X. Feng, M.-K. Song, W.C. Stolte, D. Gardenghi, D. Zhang, X. Sun, J. Zhu, E.J. Cairns, J. Guo, *Phys. Chem. Chem. Phys.*, 16 (2014) 16931-16940.
- [67] Y. Cui, S. Liu, D. Wang, X. Wang, X. Xia, C. Gu, J. Tu, *Adv. Funct. Mater.*, 31 (2021) 2006380.
- [68] NIST X-ray Photoelectron Spectroscopy Database, NIST Standard Reference Database Number 20, National Institute of Standards and Technology, Gaithersburg MD, 20899 (2000).

- [69] S.P. Lonkar, V.V. Pillai, S.M. Alhassan, *Materials Advances*, 1 (2020) 794-803.
- [70] L. Wang, T. Guo, S. Sun, Y. Wang, X. Chen, K. Zhang, D. Zhang, Z. Xue, X. Zhou, *Catal. Lett.*, 149 (2019) 1197-1210.
- [71] S. Deng, K. Zhang, D. Xie, Y. Zhang, Y. Zhang, Y. Wang, J. Wu, X. Wang, H.J. Fan, X. Xia, J. Tu, *Nano-Micro Letters*, 11 (2019) 12.
- [72] P. Luo, H. Zhang, L. Liu, Y. Zhang, J. Deng, C. Xu, N. Hu, Y. Wang, *ACS Appl. Mater. Interfaces*, 9 (2017) 2500-2508.
- [73] S.S. Zhang, J. Chen, C. Wang, *J. Electrochem. Soc.*, 166 (2019) A487-A492.
- [74] F.A. Susai, H. Sclar, S. Maiti, L. Burstein, O. Perkal, J. Grinblat, M. Talianker, S. Ruthstein, C. Erk, P. Hartmann, B. Markovskiy, D. Aurbach, *ACS Applied Energy Materials*, 3 (2020) 3609-3618.
- [75] R. Jung, M. Metzger, F. Maglia, C. Stinner, H.A. Gasteiger, *The Journal of Physical Chemistry Letters*, 8 (2017) 4820-4825.
- [76] R. Jung, M. Metzger, F. Maglia, C. Stinner, H.A. Gasteiger, *J. Electrochem. Soc.*, 164 (2017) A1361-A1377.
- [77] M.A.K.L. Dissanayake, M.A. Careem, P.W.S.K. Bandaranayake, C.N. Wijayasekera, *Solid State Ion.*, 48 (1991) 277-281.
- [78] B.T. Yu, W.H. Qiu, F.S. Li, L. Cheng, *J. Power Sources*, 158 (2006) 1373-1378.
- [79] J.-Q. Huang, Q. Zhang, H.-J. Peng, X.-Y. Liu, W.-Z. Qian, F. Wei, *Energy Environ. Sci.*, 7 (2014) 347-353.
- [80] B.-J. Chae, T. Yim, *Mater. Chem. Phys.*, 214 (2018) 66-72.

## Graphic abstract

NMC811 cathodes were conformally coated with a nanoscale  $\text{Li}_2\text{S}$  layer via atomic layer deposition (ALD). This sulfide coating was confirmed being particularly effective to protect NMC811 from structural degradation and thereby boost its electrochemical performance.

